ACS APPLIED MATERIALS & INTERFACES

www.acsami.org

Research Article

Combustion of Boron Nanoparticles Encapsulated within Perchlorate Matrices: A Mechanistic Study

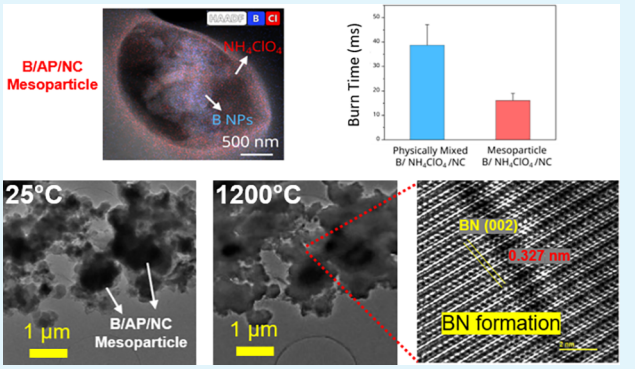
Mahbub Chowdhury, Lei Yang, Yuxin Zhou, Sammed Bhalerao, and Michael R. Zachariah*

Cite This: *ACS Appl. Mater. Interfaces* 2026, 18, 63811−63820

Read Online

ACCESS | Metrics & More | Article Recommendations | Supporting Information

ABSTRACT: Boron is an attractive high-energy fuel, but its practical combustion efficiency is limited by a viscous oxide layer that impedes oxygen transport and promotes agglomeration. Here, we address these limitations by assembling boron nanoparticles into spray-dried mesoparticles in which boron is encapsulated within an ammonium perchlorate (AP) matrix and a nitrocellulose binder. This architecture enhances fuel oxidizer proximity, accelerates AP decomposition onset by ∼60 °C, and enhances reaction kinetics as evidenced by a ∼50% pressurization rate and a ∼58% shorter burn time relative to the physically mixed formulation. In situ TEM, TGA/DSC, and T-jump time-of-flight mass spectrometry reveal that mesoparticles promote interfacial reactions producing both B_2O_3 and boron nitride (BN). BN formation is identified as a thermodynamic efficiency-loss pathway, releasing significantly less energy per mole of boron than oxidation to B_2O_3. Substituting AP with potassium perchlorate eliminates the nitrogen source, significantly reducing BN formation, and further improves combustion performance. These results demonstrate that mesoscale encapsulation combined with targeted oxidizer selection provides a practical strategy to enhance boron combustion efficiency.



KEYWORDS: *boron combustion, spray drying, ammonium perchlorate, energetics, in situ TEM, potassium perchlorate*

1. INTRODUCTION

Nanoscale metals and metalloids such as boron, aluminum, silicon, and magnesium have been explored as high-energy fuels and additives in nanoenergetic composites for propulsion applications.[1−5] Among these, boron is especially attractive because it has the highest oxidative energy density on both a gravimetric (59 kJ·g^{-1}) and volumetric basis (138 kJ·cm^{-3}).[6−8] In practice, however, boron often exhibits slow oxidation kinetics. Its native oxide, boron oxide (B_2O_3), has a relatively low melting point (∼720 K) compared with the boron core, which typically remains solid during combustion. In addition, B_2O_3 has a high boiling point (∼2130 K)[9] and forms a dense liquid layer with limited porosity, which impedes oxygen transport to the underlying boron and slows the overall oxidation process.[10−13] Reducing the particle size of metal fuels is widely used to enhance ignition sensitivity and combustion performance by shortening diffusion paths.[14] However, size reduction also increases the relative oxide content and can enhance agglomeration during combustion.[15]

One strategy to mitigate agglomeration is to assemble nanoscale components into micromter-scale mesoparticles by encapsulating them with a gas-generating polymer binder.[16−20] Encapsulation of fuel with an oxidizer or polymer can also increase the effective contact area between fuel and oxidizer, thereby improving reaction efficiency and alleviating the mass-transport limitations that often constrain physically mixed nanothermites.[21] Rapid gas generation from the polymer can deaggregate nanoparticles before or during ignition, preventing sintering and improving combustion completeness.[18] To date, however, this mesoparticle approach has been explored predominantly for aluminum-based systems.[19,22] For boron, Cheng et al. incorporated nitrocellulose (NC) and iron (Fe) particles with boron via electrospraying and showed that the oxidation temperature of B/NC/Fe composites was lower than that of neat boron, which they attributed to oxygen scavenging by iron followed by reduction by boron.[23] Hu et al. encapsulated boron in metastable intermixed composites through a self-assembly method and achieved higher combustion temperatures and shorter ignition delays.[24] In parallel, spray drying has emerged as a scalable manufacturing route for energetic

Received: July 6, 2026
Revised: October 21, 2026
Accepted: October 21, 2026
Published: November 13, 2026



Downloaded from pubs.acs.org/aamick/article-pdf/18/46/63811/6919316/am-2026-13891b.pdf by UNIV OF CALIFORNIA RIVERSIDE user on 26 November 2026

© 2026 American Chemical Society

https://doi.org/10.1021/acsami.6c13891
ACS Appl. Mater. Interfaces 2026, 18, 63811−63820

composites, enabling high production rates while producing micrometer-scale particles (~2−20 μm) with enhanced reactivity, which is advantageous for practical implementation.[16]

Ammonium perchlorate (AP) is a widely used oxidizer in solid propellants because of its strong oxidizing power and gaseous decomposition products.[25,26] Despite its common use, the interfacial reaction mechanisms between boron and AP and the extent to which intimate mixing modifies AP decomposition and boron oxidation remain insufficiently understood. In addition, competing product pathways such as boron nitride (BN) formation may consume boron without contributing effectively to useful heat release, potentially limiting overall combustion efficiency.

In this work, we have synthesized spray-dried mesoparticles in which boron nanoparticles are encapsulated within an AP matrix. 2.5 wt % NC has been added to facilitate the encapsulation of boron particles and for safety. We characterize the resulting hierarchical structure using SEM, XRD, and STEM-EDS to confirm uniform integration and nanoscale proximity between boron and oxidizer. The interfacial chemistry and thermal behavior are examined using thermogravimetric analysis, in situ TEM, and T-jump time of flight mass spectrometer, revealing that mesoparticle lowers the onset temperature and accelerates AP decomposition and promotes interfacial reactions that produce BN and B_2O_3. We then evaluate combustion performance using constant-volume combustion cell measurements and show that encapsulation substantially enhances reactivity relative to physically mixed counterparts. Finally, to understand and suppress BN formation, we replace AP with potassium perchlorate (KP) and fabricate analogous B/KP/NC mesoparticles. By comparing AP- and KP-based systems, we elucidate how oxidizer chemistry and decomposition pathways influence interfacial product formation and macroscopic combustion performance.

2. MATERIALS AND METHODS

2.1. Materials/Sample Preparation

Nanoscale boron (~100 nm, 80% active) was purchased from US Research Nanomaterials Inc. Ammonium perchlorate (200 nm) was purchased from Pyro chemical Source LLC. Potassium perchlorate was purchased from Sigma-Aldrich. Nanoscale AP and KP were synthesized via an aerosol spray pyrolysis (ASP) approach from as-received powders.[27,28] Generally, 1 g of as-purchased larger particles was dissolved into 100 mL of deionized water, and the obtained solution was sprayed into small droplets with an atomizer operating at ~35 psi using compressed air. The droplets passed through a silica-gel diffusion drier to remove water and sequentially passed through a tube furnace that operated at 150 °C. The final product was collected on filter paper. The average particle size from ASP was found to be ~400 nm. A collodion solution (4−8% in ethanol/diethyl ether) was obtained from Millipore Sigma and was dried to obtain solid nitrocellulose for further processing.

2.2. Spray Drying

To prepare the formulations for spray drying, a stoichiometric amount of AP or KP was added with B assuming complete B_2O_3 formation as shown below. Note that BN formation was not expected initially when the sample was made but will be addressed later in the paper.

$$10B + 6NH_4ClO_4 \rightarrow 5\,B_2O_3 + 9H_2O + 6HCl + 3N_2 \quad (1)$$

$$8B + 3KClO_4 \rightarrow 4\,B_2O_3 + 3\,KCl \quad (2)$$

The desired amount of NC binder was dissolved in a 3:5:2 DMF:IPA:acetone solvent mixture. Boron nanoparticles were then added to the solution according to stoichiometry. The suspension was then sonicated for ~1 h, followed by a minimum of 24 h of stirring. The slurry was then shear mixed and sonicated during the process of spray drying to enable homogeneous particle mixing throughout the suspension. For spray drying the formulations, a Büchi B-290 mini spray dryer was used in conjunction with a B-295 inert loop. Argon preheated at ~110 °C was used as the drying gas throughout the spray drying system. The schematic of spray drying is shown in Figure 1. The prepared suspension was fed through a peristaltic pump at a 45% feeding rate (~12.5 mL min^{-1}) with an aspirator rate of 85% (~33 $m^3\,h^{-1}$) and ~7 L min^{-1} of inlet gas flow. The particles were collected in a cyclone-based collector, which was electrostatically neutralized before sample collection. For the safe handling of materials, low solid loading (10 mg mL^{-1}) was used while formulating the precursor solutions.

2.3. Conventional Physical Mixing

To prepare the physical mixtures, the NC solution (20 mg mL^{-1}, 0.7:1 DMF:acetone solvent mixture) was first spray dried at a drying

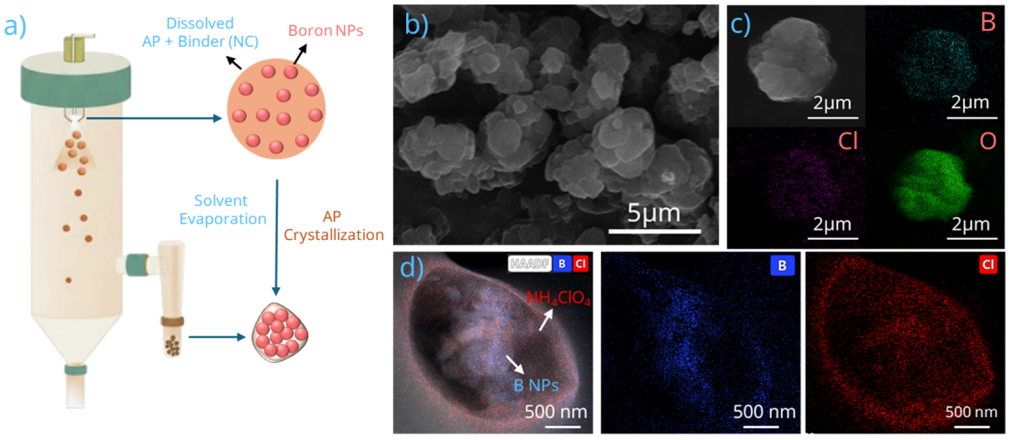


Figure 1. (a) Schematic illustration of the spray-drying synthesis strategy employed to fabricate B/AP/NC mesoparticles. (b) SEM image showing the spherical morphology of the synthesized mesoparticles. (c) SEM-EDS elemental maps of a single mesoparticle confirming a homogeneous distribution of B, Cl, and O. (d) HAADF-STEM image and corresponding EDS elemental maps revealing boron nanoparticle cores encapsulated within the crystalline NH_4ClO_4 matrix; electron-beam induced exposure reduced matrix density, enabling visualization of the encapsulated boron particles.

Downloaded from pubs.acs.org/aamick/article-pdf/18/46/63811/6913516/am-2026-13891b.pdf by UNIV OF CALIFORNIA RIVERSIDE user on 26 November 2026

https://doi.org/10.1021/acsami.6c13891
ACS Appl. Mater. Interfaces 2026, 18, 63811−63820

temperature of 110 °C to obtain the NC powder. The NC powder was then mixed with B and size reduced AP and KP in hexane following stoichiometric eqs 1 and 2, followed by sonication for ∼1 h and drying overnight to obtain physically mixed B/AP/NC or B/KP/NC powders.

2.4. In Situ Transmission Electron Microscopy

In situ experimentation was conducted on a Thermo Fisher Scientific (FEI Titan Themis 300) operating at 300KV utilizing a Protochips Fusion Holder in a vacuum chamber maintained at 10^{-7} Torr. The synthesized mesoparticles from the spray dryer were sonicated in hexane for dispersion and then drop-casted onto the heating membrane supported by carbon films. The e-chip used in these experiments has been calibrated by Protochips to maintain 5% temperature accuracy and uniform heating across the entire heating membrane. The TEM alignments were conducted previously in a blank chip to minimize beam-induced artifacts, and the sample was quickly heated at a rate of 200 °C·s^{-1} from room temperature to 1200 °C to decouple the effect of the beam. HRTEM was performed to identify the phase formation upon reaction. High-angle annular dark field (HAADF) imaging, and EDS elemental mapping was performed for compositional analysis. The molar ratio of the comparable fraction of BN and B_2O_3 formation was quantified using Velox software.

2.5. Time of Flight Mass Spectrometry (TOF-MS)

Temperature jump time-of-flight mass spectrometry (T-jump TOFMS) was used for in situ time- and temperature-resolved identification of the gas phase species released during the preignition and combustion reactions. Details about the mass spectrometer can be found in several of our previous publications.[29−32] For this measurement, a thin Pt wire (∼75 μm) is used as the sample holder, on which thin layers of solid nanopowder samples are coated by drop-casting through micropipets. During the measurement, the Pt wire is resistively heated to ∼1500 K by applying a voltage pulse of width ∼3 ms, which leads to an average heating rate of $\sim 5 \times 10^5$ K s^{-1}. The thin coating of the sample ensures that the sample is at the same instantaneous temperature as that of the wire and that it is uniformly heated at the same heating rate. Through a probe, the current across the wire is monitored at every 0.1 ms, and the Callendar−Van Dusen equation is used to estimate the instantaneous wire temperature at every 0.1 ms over the 3 ms pulse. The gas phase species released on thermal activation of the reactions are sampled and identified over 10 ms at an interval of 0.1 ms by the time-of-flight mass spectrometric process. This measurement is performed under a high vacuum of $\sim 10^{-10}$ atm.

2.6. Combustion Cell Characterization

Constant-volume combustion cell measurements were performed to characterize the pressurization rate and burn time of the self-propagating combustion reaction. For each measurement, 25 mg of the stoichiometric formulation was loaded loosely into a ∼20 cm^3 chamber sealed in ambient air at atmospheric pressure. The sample was ignited at the center of the powder-bed surface by the tip of a resistively heated nichrome wire, which contacted the surface without being embedded in the powder. Time-resolved pressure and optical emission were recorded simultaneously using a PCB piezoelectric pressure transducer and a Hamamatsu photomultiplier tube, respectively. Peak pressure and pressurization rate were extracted from the pressure trace, and burn time was defined as the full width at half maximum of the optical-emission signal. At least four measurements were performed for each formulation. Further details of the measurement can be found in previous work from our group.[33,34]

2.7. Single Particle Combustion Studies

To observe the burning behavior of B/AP/NC mesoparticles, a methane/oxygen/nitrogen diffusion flame burner (Hencken type) combined with intensified microscopic imaging techniques was employed. A more detailed description can be found in our previous work.[35] Aerosolized B/AP/NC mesoparticles were delivered into the post-flame region of a fuel-lean methane/oxygen/nitrogen flame and their burning trajectories were recorded by a high-speed camera (Vision Research Phantom VEO710L) coupled with a long working distance microscope objective (Infinity Photo-Optical Model K2 DistaMax). Control experiments were performed under identical conditions on AP alone, boron nanoparticles alone, and physically mixed B/AP/NC.

2.8. Material Characterization (SEM, XRD, and TGA-DSC)

A Thermo-Fisher Scientific FEI NNS450 scanning electron microscope, operating at 18 kV, was used to characterize the morphology and the size of the microparticles. SEM energy-dispersive spectroscopy was used to evaluate the elemental homogeneity of the microparticles. SEM images using ImageJ software (v. 1.53) were used to extract particle size distributions with a nominal sample size of 50 mesoparticles. X-ray diffraction (XRD) was performed using a PANalytical Empyrean Series 2 diffractometer under Cu Kα radiation to investigate the crystallinity and composition of the samples. TGA-DSC measurements were carried out using a NETZSCH STA 449 F3 Jupiter thermogravimetric analyzer on alumina pans, with a temperature ramp rate of 10 K·min^{-1} up to a final temperature of 773 K, under an argon flow of 50 mL·min^{-1}. Roughly 1 mg of sample was used for each run for safety reasons.

3. RESULTS AND DISCUSSION

3.1. Mesoparticle Synthesis

The spray-drying synthesis process leverages differential solubility and crystallization kinetics. Boron nanoparticles were dispersed in DMF containing dissolved ammonium perchlorate (AP) and nitrocellulose (NC) binder (2.5 wt %). Upon atomization through the spray-dryer nozzle, rapid solvent evaporation induced AP supersaturation, which drove crystallization around the insoluble boron phase. This resulted in a continuous oxidizer matrix embedding the fuel nanoparticles (Figure 1a). The resulting mesoparticles exhibited a narrow size distribution ranging from 1−5 μm with a mean diameter of ∼3.2 μm (Figure 1b and Figure S1). Scanning electron microscopy coupled with energy-dispersive X-ray spectroscopy (SEM-EDS) confirmed intimate fuel-oxidizer integration as evidenced by uniform distribution of B, Cl, and O signals across individual mesoparticles (Figure 1c).

High-angle annular dark-field scanning transmission electron microscopy (HAADF-STEM) with EDS mapping provided direct visualization of the hierarchical nano-microstructure (Figure 1d). Interestingly, under electron-beam irradiation, the AP matrix became more electron-transparent, likely due to beam-induced decomposition and mass loss. This enhanced contrast enabled the visualization of encapsulated boron nanoparticle cores within the continuous AP matrix, further confirming the high degree of fuel-oxidizer proximity.

3.2. Thermal Analysis- Effect on AP Decomposition

To characterize the thermal behavior of the mesoparticles under slow heating, TGA/DSC was performed on B/AP/NC mesoparticles, the physically mixed counterpart, an AP/B_2O_3 mixture, and size-reduced AP. AP decomposition is commonly divided into two stages: a low-temperature stage (LTS) and a high-temperature stage (HTS). During the LTS, AP decomposes via a surface-mediated proton-transfer process, producing NH_3 and $HClO_4$.[36]

Downloaded from pubs.acs.org/aamick/article-pdf/18/46/63811/6913516/am-2026-13891b.pdf by UNIV OF CALIFORNIA RIVERSIDE user on 26 November 2026

https://doi.org/10.1021/acsami.6c13891
ACS Appl. Mater. Interfaces 2026, 18, 63811−63820

We begin by discussing the slow-heating TGA/DSC results shown in Figure 2. As a reference, we first characterized the as-synthesized size reduced AP (Figure 2a,b-iv). An endotherm at ~240 °C corresponds to the orthorhombic-to-cubic phase transition. Upon further heating, an exotherm at ~273 °C is observed, corresponding to the LTS. A second endotherm at ~380 °C follows, associated with the HTS, during which NH_3 and $HClO_4$ undergo further decomposition to generate additional gaseous products, including H_2O, N_2O, NO/NO_2, HCl, and Cl_2. Prior studies suggest that AP exhibits a competition between sublimation (endothermic) and thermal decomposition (exothermic).[37] In our measurements, AP decomposition was complete by ~400 °C (Figure 2a-iv).

The AP/B_2O_3 mixture (Figure 2a,b-iii) did not show additional thermal features, indicating minimal interactions between these components under the conditions tested. The physically mixed B/AP/NC sample (Figure 2a,b-ii) did not exhibit the initial LTS exotherm; instead, there was a broad endotherm observed at 320 °C, occurring at a significantly lower temperature than that of size reduced AP alone. This shift likely reflects earlier onset of AP decomposition facilitated by heat generated from B/AP interfacial reactions. The broad endothermic character suggests that decomposition proceeded with relatively slow kinetics, with sublimation dominating over exothermic decomposition pathways. Additionally, given that NC constitutes only 2.5 wt % of the system and decomposes at ~180 °C, no distinct thermal signature attributable to NC decomposition was resolved in the DSC trace.

By contrast, the B/AP/NC mesoparticles (Figure 2a,b-i) demonstrated significantly enhanced reactivity. AP decomposition initiated ~60 °C earlier than in both neat AP and the physically mixed sample, with completion at ~335 °C, ~50 °C earlier than the physically mixed counterpart. Interestingly, the most significant change was the disappearance of the second endothermic peak and the appearance of an exotherm at ~350 °C, indicating that the mesoparticle directly facilitates exothermic decomposition.

To further probe the B-AP interactions, solid residues collected at ~400 °C from the TGA experiments were analyzed by XRD (Figure S2). The diffraction patterns confirmed the formation of BN and H_3BO_3. Both products arise from exothermic reactions and can contribute additional heat to accelerate AP decomposition.[38,39] In this system, BN formation may proceed via reaction of boron with AP decomposition products such as N_2 and NH_3 according to eqs 3 and 4.

$$B(s) + \tfrac{1}{2}\,N_2\,(g) \rightarrow BN\,(s)\ \Delta H = -250.9\ \text{kJ mol}^{-1} \quad (3)$$

$$B(s) + NH_3\,(g) \rightarrow BN\,(s) + 3/2\,H_2\,(g)\ \Delta H = -209\ \text{kJ mol}^{-1} \quad (4)$$

On the other hand, boron can be oxidized by oxygen containing species generated during AP decomposition to form B_2O_3 (eq 5), which upon exposure to ambient moisture converts to H_3BO_3 (eq 6).[38]

$$B\,(s) + \tfrac{3}{4}\,O_2 \rightarrow \tfrac{1}{2}\,B_2O_3\ \Delta H = -637\ \text{kJ mol}^{-1} \quad (5)$$

$$B_2O_3(s) + 3H_2O\,(l) \rightarrow 2H_3BO_3\,(s)\ \Delta H = -57.6\ \text{kJ mol}^{-1} \quad (6)$$

Collectively, these results indicate that intimate encapsulation of boron nanoparticles within the AP matrix enhances interfacial mass transport and heat transfer, thereby accelerating

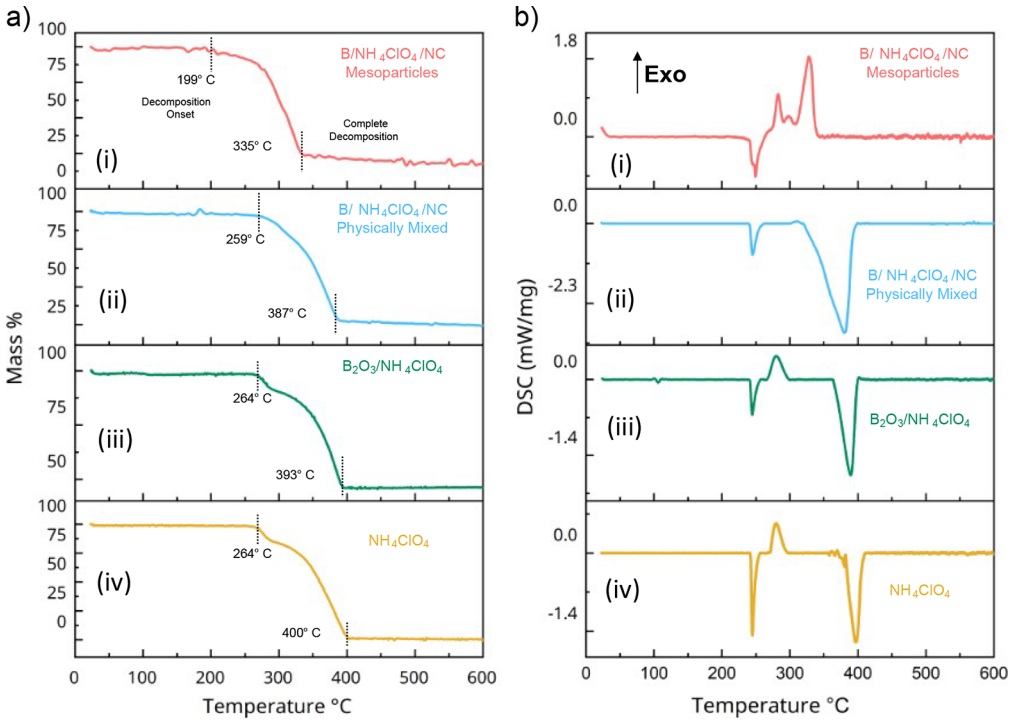


Figure 2. (a) TGA and (b) DSC curves obtained under slow heating conditions for (i) B/NH_4ClO_4/NC mesoparticles, (ii) physically mixed B/NH_4ClO_4/NC, (iii) NH_4ClO_4/B_2O_3 mixture, and (iv) size-reduced NH_4ClO_4, demonstrating that encapsulation of boron nanoparticles within the NH_4ClO_4 matrix enhances decomposition.

https://doi.org/10.1021/acsami.6c13891
ACS Appl. Mater. Interfaces 2026, 18, 63811−63820

Downloaded from pubs.acs.org/aamick/article-pdf/18/46/63811/6913516/am-2026-13891b.pdf by UNIV OF CALIFORNIA RIVERSIDE user on 26 November 2026

decomposition kinetics and advancing the overall reaction progression to lower temperatures.

3.3. In Situ TEM Rapid Heating

To understand and directly visualize the reactive interactions within the B/AP/NC mesoparticles, we performed *in* situ TEM heating experiments under vacuum to decouple gas-phase effects. Samples were heated from 25 to 1200 °C at 200 °C·s^{-1}. Since AP is susceptible to electron-beam-induced degradation,[40] all microscope alignments were completed prior to insertion of the heating holder. The elevated heating rate was additionally employed to minimize beam exposure during the experiment.

Figure 3a,d shows that upon heating and AP decomposition, the internal morphology of the mesoparticles was revealed, with boron nanoparticles confined within the particle core. Atomic-resolution imaging in Figure 3b,c acquired after heating showed the in situ nucleation of boron nitride (BN), evidenced by a measured lattice spacing of 0.327 nm consistent with the dominant BN (002) plane. STEM-EDS (Figure 3e,f) analysis performed on multiple particles indicated that the condensed reaction products contained comparable fractions of BN and B_2O_3, with a BN:B_2O_3 molar ratio of 0.49:0.51.

We evaluated the standard Gibbs free energies for two limiting overall pathways in which boron reacts with ammonium perchlorate decomposition products to form either B_2O_3 or BN. Calculations show (Figure S3) that both B_2O_3 and BN formation are thermodynamically spontaneous across the entire range examined in TEM. The calculations indicate that the B_2O_3 forming pathway is more favorable at lower temperature, whereas BN formation is increasingly competitive at higher temperature due to large entropy gain since BN formation path produced more gaseous products per mole of boron consumed (S3), yielding a crossover at ~900 °C. This trend is consistent with STEM EDS showing comparable fractions of BN and B_2O_3 after heating to 1200 °C, suggesting that both oxidation and nitridation pathways can be operative during the reaction. We note that the product distribution measured here is specific to the vacuum rapid-heating environment. Under a closed combustion chamber, gaseous decomposition products remain available for secondary reaction with boron, and the relative proportions of BN and B_2O_3 may differ accordingly.

3.4. Mechanism Underlying the Reactive Characteristics

T-Jump/TOFMS measurements were employed to probe the reaction mechanism at an ultrafast heating rate of ~5 × 10^5 °C·s^{-1}. Figure 4a compares the average mass spectra of physically mixed B/AP/NC and the encapsulated B/AP/NC mesoparticles. Major peaks were observed at m/z 16 (O^+), 32 (O_2^+), 36.5 (HCl^+), 51.5 (ClO^+), 83.5 (ClO_3^+), 43 (BO_2^+), 44 (HBO_2^+, N_2O+), 46 (BCl^+, NO_2^+), and 69 ($B_2O_3^+$). Yeh and Kuo reported that major boron-oxygen reaction products include HOBO and BO_2.[8] Ao et al. reported B_2O_3 as a primary combustion product of boron-containing propellants.[41] Consistent with these studies, our results show that the BO_2 and HBO_2 signals are prominent in the B/AP/NC mesoparticle spectrum, whereas they are negligible for the physically mixed formulation.

Time-resolved temporal profiles further highlight differences in reaction progression. For m/z = 44 (Figure 4b), the physically mixed sample exhibits a small peak near ~240 °C, which may correspond to N_2O formation or

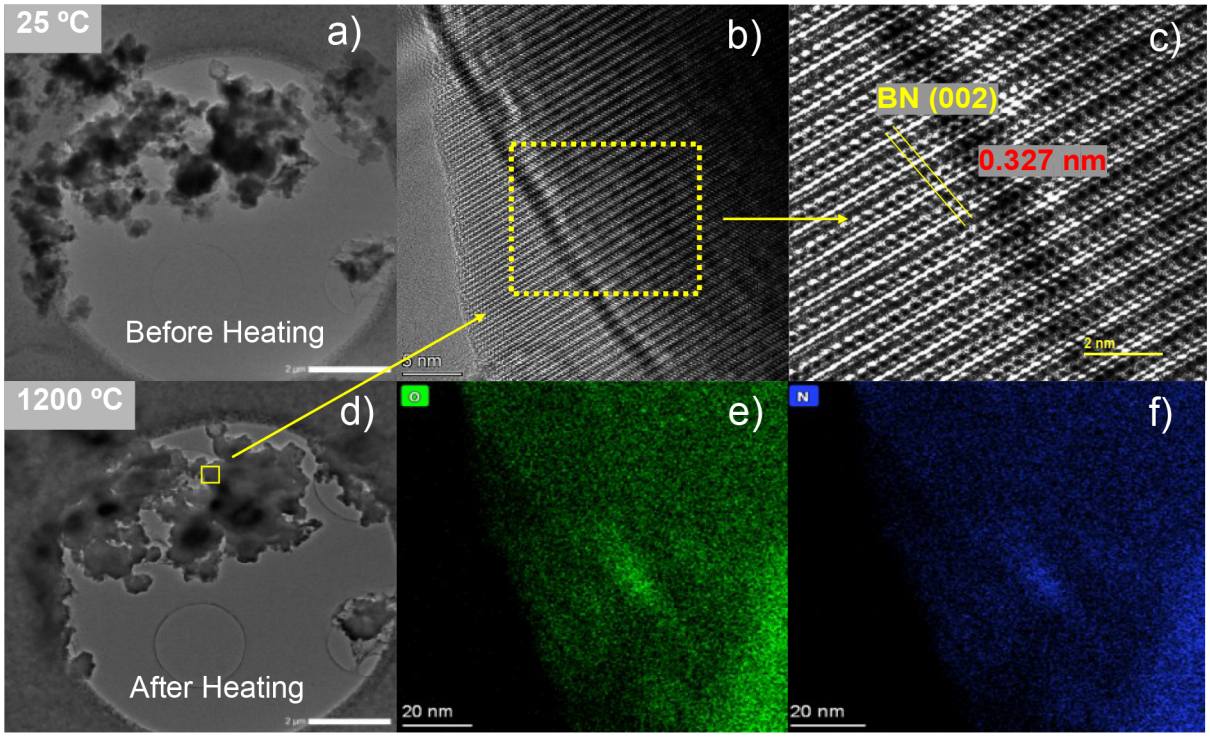


Figure 3. In situ TEM heating of a B/AP/NC mesoparticle under vacuum at a heating rate of 200 °C·s^{-1} (a) before heating and (d) after heating to 1200 °C, revealing boron nanoparticle cores following AP decomposition. (b, c) Atomic-resolution images acquired after heating, confirming in situ BN formation. (e, f) Corresponding STEM−EDS elemental maps showing the spatial distribution of O and N in the post-reaction products.

https://doi.org/10.1021/acsami.6c13891
ACS Appl. Mater. Interfaces 2026, 18, 63811−63820

Downloaded from pubs.acs.org/journal/article-pdf/18/46/63811/6913516/am-2026-13891b.pdf by UNIV OF CALIFORNIA RIVERSIDE user on 26 November 2026

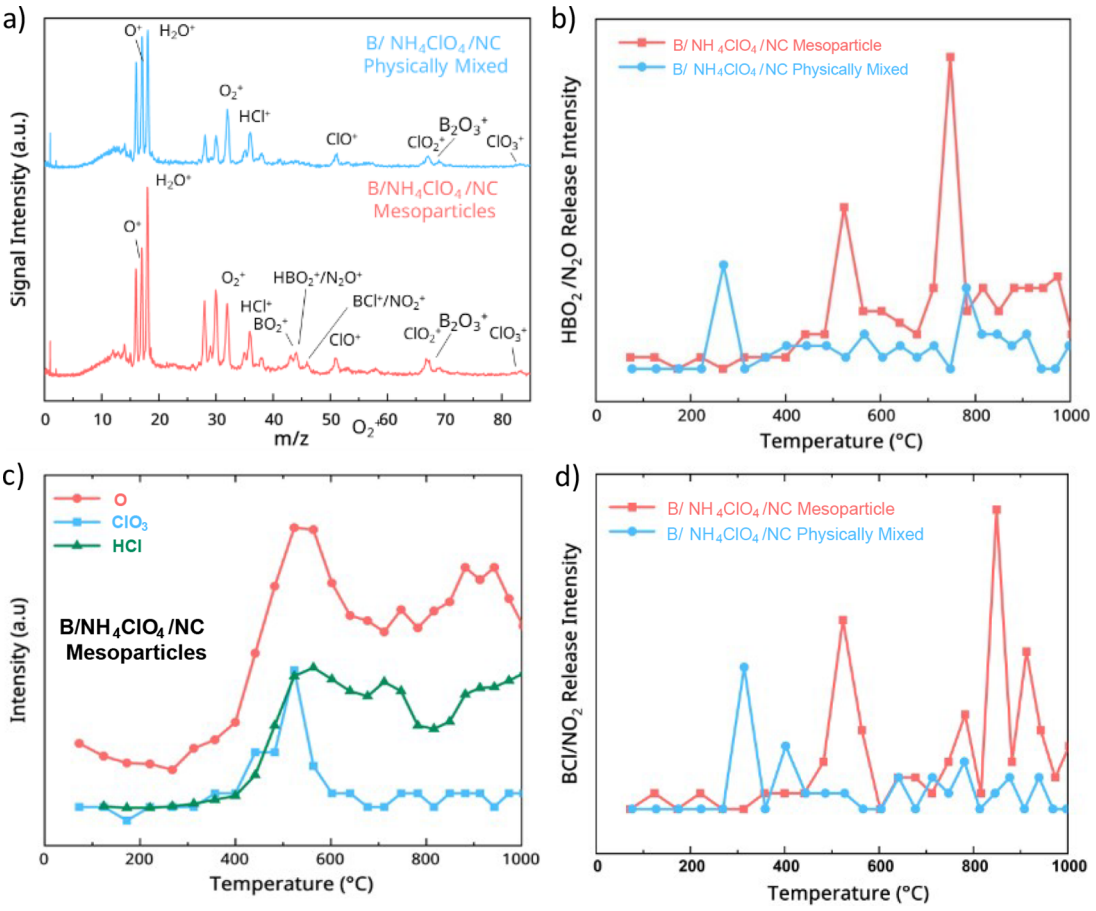


Figure 4. T-jump/TOFMS results comparing physically mixed B/AP/NC and encapsulated B/AP/NC mesoparticles. (a) Average mass spectra showing enhanced formation of boron-containing reaction products. (b) Time-resolved release of HBO_2/N_2O ($m/z = 44$). (c) Time-resolved evolution of AP decomposition products. (d) Time-resolved signal for $m/z = 46$, corresponding to BCl/NO_2 release.

CO_2 near the NC decomposition temperature. Given its lower decomposition temperature, any contribution from NC would be confined to the low-temperature region. A second feature near ~500 °C is consistent with N_2O production associated with AP decomposition, aligning with the release temperatures of other AP-derived species discussed below. At higher temperatures (~700 °C), a distinct signal attributable to boron-containing HBO_2 is observed, but it remains minimal for the physically mixed sample.

From AP decomposition products (Figure 4c), oxygen evolution appears near ~300 °C, consistent with the low-temperature stage (LTS). Additional major products, including HCl and ClO_3, emerge near ~500 °C, corresponding to the high-temperature stage (HTS). In the average spectra (Figure 4a), these AP-derived signals exhibit higher intensities for the mesoparticle sample than for the physically mixed sample, indicating a more complete oxidizer decomposition. Collectively, these results suggest that intimate encapsulation promotes more complete boron/oxidizer reactions.

Further evidence for boron-chlorine chemistry is provided by $m/z = 46$ (Figure 4d). At lower temperatures, this signal is consistent with NO_2 formation from AP/NC decomposition. At higher temperatures (~850 °C), the appearance of BCl^+ commonly produced by electron-impact fragmentation of BCl_3,[42] which also coincides with HBO_2 production. This temporal overlap supports a high-temperature interaction pathway involving the boron oxide layer and chlorine-containing oxidizer decomposition products.

3.5. Effect of Mesoparticle Architecture on Combustion Kinetics

The reactivity and combustion characteristics of the B/AP/NC mesoparticles were evaluated using constant-volume combustion cell measurements. Samples (25 mg) at stoichiometric composition were ignited and a fast-response pressure transducer coupled with an optical emission sensor was used to extract peak pressure, pressurization rate, and burn time (Figure 5a–c). Raw pressure and optical emission traces are shown in Figure S4. The mesoparticle formulation exhibited markedly enhanced reactivity relative to the physically mixed sample, producing higher peak pressures and pressurization rates and shorter burn times. The peak pressure increased by ~50%, pressurization rate by ~53% and burn time decreased by 58%, indicating that encapsulation substantially enhances reaction kinetics. Post-combustion SEM images (Figure S5a,b) show pronounced differences in residue morphology, the average residue particle size for the physically mixed sample was ~200 μm, whereas the mesoparticle residue averaged ~10 μm, corresponding to ~20-fold reduction in agglomeration during combustion (Figure S5c).

High-speed microscopy (Figure 5d–g) performed on individual B/AP/NC mesoparticles in the post-flame region of a

https://doi.org/10.1021/acsami.6c13891
ACS Appl. Mater. Interfaces 2026, 18, 63811–63820

Downloaded from pubs.acs.org/aamick/article-pdf/18/46/63811/6913516/am-2026-13891b.pdf by UNIV OF CALIFORNIA RIVERSIDE user on 26 November 2026

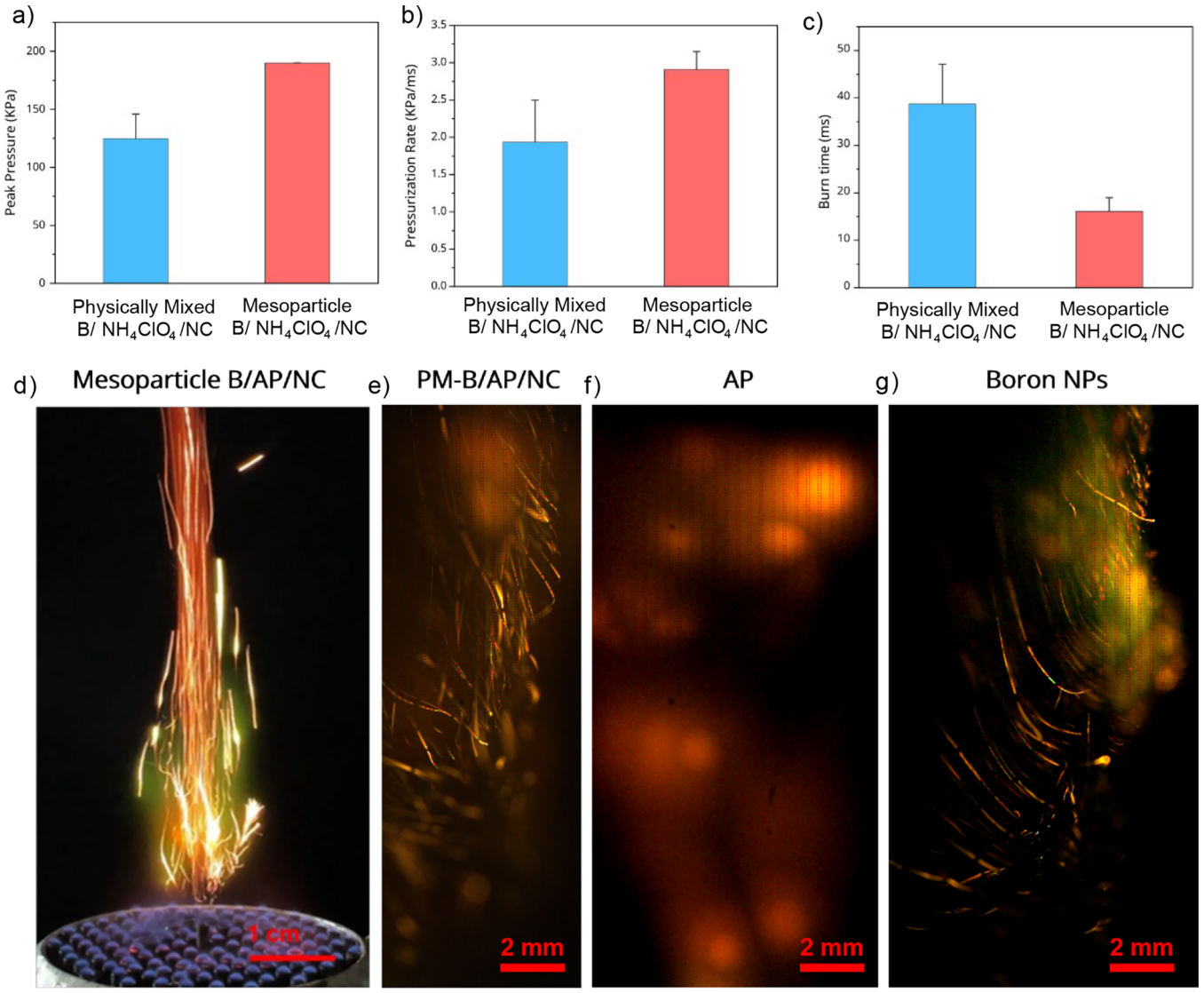


Figure 5. Constant-volume combustion-cell measurements comparing physically mixed B/AP/NC (blue) and B/AP/NC mesoparticles (red): (a) peak pressure, (b) pressurization rate, and (c) burn time. Error bars represent the standard deviation of at least four measurements. (d) Wide view of B/AP/NC mesoparticle combustion in the post-flame region of a fuel-lean $CH_4/O_2/N_2$ flame. High-speed images under the same conditions of (e) physically mixed B/AP/NC, (f) AP alone, and (g) boron nanoparticles.

Hencken Burner operating under fuel-lean $CH_4/O_2/N_2$ conditions shows that mesoparticles exhibited microexplosion behavior in which individual mesoparticles disintegrated into multiple luminous subparticles. Under the same conditions, AP alone produced diffuse emission without discrete particle trajectories (Figure 5f), and boron nanoparticles produced green emission (Figure 5g), commonly attributed to BO_2, with largely straight trajectories. The physically mixed sample shows largely straight burning trajectories, whereas the mesoparticles show firework-like fragmentation. The physically mixed sample (Figure 5e) appears to resemble a superposition of the separate AP and boron burning behaviors, which may indicate weaker interaction between boron and AP when they are not intimately mixed. These observations are consistent with the constant-volume combustion results, in which the post-combustion residue of the mesoparticles was approximately 20-fold smaller than that of the physically mixed sample (Figure S5). Together, these results suggest that microexplosions may help limit sintering and promote more complete reaction.

Post-combustion residues from constant-volume combustion were also collected for XRD analysis (Figure 6a,b). The physically mixed sample contained substantial unreacted AP alongside condensed-phase products consistent with BN and H_3BO_3. The presence of H_3BO_3 is expected as B_2O_3 is hygroscopic and readily absorbs moisture.[38] In contrast, the mesoparticle residue contained only BN and H_3BO_3, with no detectable unreacted AP. This indicates that AP decomposed more completely within the encapsulated formulation. This enhanced conversion is consistent with localized heat generation and the higher overall reactivity of the mesoparticles, suggesting improved combustion efficiency. In our system, AP also acts as an effective gas generator, and NC can promote AP deflagration.[43] The combined gas generation helps mitigate sintering. Notably, the physically mixed sample contained the same

Downloaded from pubs.acs.org/aamick/article-pdf/18/46/63811/6919316/am-2026-13891b.pdf by UNIV OF CALIFORNIA RIVERSIDE user on 26 November 2026

https://doi.org/10.1021/acsami.6c13891
ACS Appl. Mater. Interfaces 2026, 18, 63811−63820

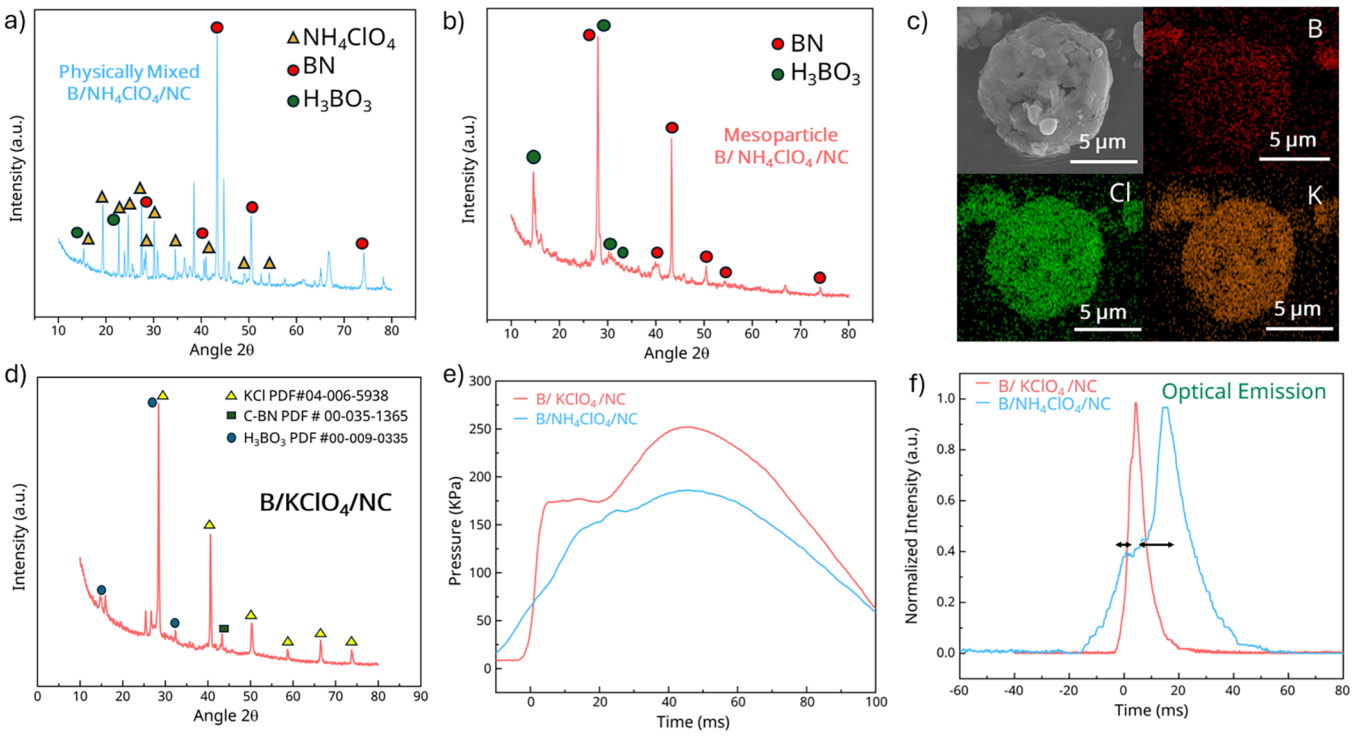


Figure 6. XRD patterns of the post-combustion products from B/AP/NC: (a) physically mixed; (b) mesoparticle showing a more complete reaction in the mesoparticle formulation. (c) SEM/EDS elemental maps of B/KP/NC mesoparticles confirming homogenous distribution of B, K, and Cl. (d) XRD patterns of post-combustion products from B/KP/NC mesoparticles showing minimal BN formation. (e, f) Constant-volume combustion-cell pressure traces and optical-emission profiles comparing AP- and KP-based mesoparticle systems.

quantity of NC loading. The spatial confinement of boron nanoparticles within the AP matrix facilitates rapid interfacial reaction kinetics and promotes complete AP decomposition.

3.6. Role of Nitrogen Source in BN Formation

As described earlier, XRD analysis of post-combustion products revealed substantial BN formation. Given that the system contains both NC and NH_4ClO_4 as potential nitrogen source and that constant-volume combustion was conducted under ambient conditions with residual N_2 present. This origin of BN formation needs careful consideration. From a thermodynamically standpoint, if Boron reacts with AP to form either B_2O_3 or BN, the per mole heat release is significantly higher for oxidation pathway (eq 7) than for the nitridation pathway (eq 8)

$$10B\ (s) + 6NH_4ClO_4\ (s) \rightarrow 5B_2O_3\ (s) + 6HCl\ (g) + 3N_2\ (g) + 9H_2O\ (l)\ \Delta H = -771.92\ kJ/molB \quad (7)$$

$$4B\ (s) + 4NH_4ClO_4\ (s) \rightarrow 4BN\ (s) + 4HCl\ (g) + 6H_2O\ (l) + 5O_2\ (g)\ \Delta H = -476.20\ kJ/molB \quad (8)$$

BN formation is therefore thermodynamically less favorable on an energy-release basis and is expected to reduce the overall combustion efficiency of the system. To isolate the role of nitrogen in BN formation, the AP oxidizer was substituted with potassium perchlorate (KP), and B/KP/NC mesoparticles were synthesized (Figure 6c). The resulting particle size distribution (Figure S6) was comparable to the AP-based system, with an average particle size of ∼5 μm. SEM-EDS mapping confirmed a homogeneous distribution of B, Cl, and K throughout individual mesoparticles.

These mesoparticles were ignited in the constant-volume combustion chamber, and post-combustion products were analyzed by XRD (Figure 6d). The diffraction patterns were dominated by KCl, consistent with $KClO_4$ decomposition, along with H_3BO_3 formation. Crucially, only a trace amount of BN was detected, significantly less than in the AP system. Since the NC loading is unchanged between the two formulations, this identifies AP as the dominant nitrogen source, with the residual BN consistent with a secondary contribution from NC decomposition.

When normalized by the total mass of the stoichiometric B/oxidizer formulation, the calculated heat release of the $B/KClO_4$ system is only ∼7% higher than that of the B/NH_4ClO_4 system, assuming complete conversion of boron to B_2O_3 (S8). However, from our combustion cell experiment the pressurization rate increased by ∼8×, and the peak pressure was ∼35% higher for the KP system (Figure 6e). The KP mesoparticle system exhibited a burn time of ∼6 ms, compared to ∼14 ms for the AP mesoparticle system, indicating a substantial improvement in reaction rate (Figure 6f). Unlike AP, $KClO_4$ is not an effective gas generator and decomposes primarily to KCl and O_2. Consequently, SEM analysis of the post-combustion residues revealed significant agglomeration (Figure S7). However, the KP mesoparticle system outperformed the AP-based system in constant-volume combustion, underscoring the importance of suppressing BN formation as a strategy to improve overall combustion efficiency.

Downloaded from pubs.acs.org/aamick/article-pdf/18/46/63811/6913516/am-2026-13891b.pdf by UNIV OF CALIFORNIA RIVERSIDE user on 26 November 2026

https://doi.org/10.1021/acsami.6c13891
ACS Appl. Mater. Interfaces 2026, 18, 63811−63820

CONCLUSIONS

In this work, we demonstrate a scalable spray-drying approach to fabricate boron-based energetic mesoparticles in which boron nanoparticles are uniformly encapsulated within an ammonium perchlorate matrix. This architecture accelerates fuel-oxidizer proximity, accelerating AP decomposition onset by ∼60 °C. Constant-volume combustion experiments showed substantially enhanced reactivity with single particle imaging revealed a microexplosion mechanism that suppresses agglomeration and promotes reaction conversion. However, the AP-based system also favors formation of boron nitride, which represents an efficiency loss pathway for boron utilization. Substituting AP with potassium perchlorate suppressed BN formation and yielded an ∼8× increase in pressurization rate confirming oxidizer decomposition chemistry is critical for energy release efficiency in composite energetic system. Overall, these findings provide design principles for boron-based propellants, in which oxidizer chemistry and encapsulation architecture can be tuned independently to maximize boron utilization.

ASSOCIATED CONTENT

Supporting Information

The Supporting Information is available free of charge at https://pubs.acs.org/doi/10.1021/acsami.6c13891.

Particle size distribution of spray-dried B/AP/NC mesoparticles; XRD of the TGA product of B/AP/NC mesoparticles; Gibbs free energy calculation for BN and B_2O_3 formation; combustion-cell pressure traces and optical-emission profile; SEM images and size distribution of post-combustion residues from physically mixed and mesoparticle B/AP/NC; particle size distribution of spray-dried B/KP/NC mesoparticles; heat release comparison between B/AP and B/KP systems; SEM of post-combustion products of physically mixed and mesoparticle B/KP/NC (DOCX)

AUTHOR INFORMATION

Corresponding Author

Michael R. Zachariah − *Departments of Chemical and Environmental Engineering, University of California, Riverside, California 92521, United States;* orcid.org/0000-0002-4115-3324; Email: mrz@engr.ucr.edu

Authors

Mahbub Chowdhury − *Departments of Chemical and Environmental Engineering, University of California, Riverside, California 92521, United States*

Lei Yang − *Departments of Chemical and Environmental Engineering, University of California, Riverside, California 92521, United States;* orcid.org/0000-0002-1094-8642

Yuxin Zhou − *Departments of Chemical and Environmental Engineering, University of California, Riverside, California 92521, United States;* orcid.org/0009-0005-1397-3834

Sammed Bhalerao − *Departments of Chemical and Environmental Engineering, University of California, Riverside, California 92521, United States;* orcid.org/0009-0000-4792-6714

Complete contact information is available at: https://pubs.acs.org/doi/10.1021/acsami.6c13891

Author Contributions

M.C.: Conceptualization, Investigation, Writing-Original Draft, Methodology, Visualization, Formal Analysis. L.Y.: Conceptualization, Investigation, Writing- Original Draft, Methodology, Visualization, Formal Analysis. Y.Z.: Methodology, Investigation. S.B.: Investigation. M.R.Z.: Conceptualization, Writing − review & editing, Supervision, Resources, Project administration, Methodology, Funding acquisition.

Notes

The authors declare no competing financial interest.

ACKNOWLEDGMENTS

This work was supported by the AFOSR and NSF.

REFERENCES

(1) Jiang, Y.; Deng, S.; Hong, S.; Zhao, J.; Huang, S.; Wu, C.-C.; Gottfried, J. L.; Nomura, K.; Li, Y.; Tiwari, S.; Kalia, R. K.; Vashishta, P.; Nakano, A.; Zheng, X. Energetic Performance of Optically Activated Aluminum/Graphene Oxide Composites. *ACS Nano* **2018**, *12* (11), 11366−11375.

(2) Dreizin, E. L. Metal-Based Reactive Nanomaterials. *Prog. Energy Combust. Sci.* **2009**, *35* (2), 141−167.

(3) Ghildiyal, P.; Biswas, P.; Herrera, S.; Xu, F.; Alibay, Z.; Wang, Y.; Wang, H.; Abbaschian, R.; Zachariah, M. R. Vaporization-Controlled Energy Release Mechanisms Underlying the Exceptional Reactivity of Magnesium Nanoparticles. *ACS Appl. Mater. Interfaces* **2022**, *14* (15), 17164−17174.

(4) Xu, F.; Nava, G.; Biswas, P.; Dulalia, I.; Wang, H.; Alibay, Z.; Gale, M.; Kline, D. J.; Wagner, B.; Mangolini, L.; Zachariah, M. R. Energetic Characteristics of Hydrogenated Amorphous Silicon Nanoparticles. *Chem. Eng. J.* **2022**, *430*, No. 133140.

(5) Zhang, C.; Kou, Y.; Xiao, L.; Hu, Y.; Lu, Q.; Zhao, F.; Hu, Y.; Jiang, W.; Yang, Y.; Hao, G. Research Progress on the Modification of B and Al High-Energy Fuels for Powder Fuel Ramjet Applications. *ACS Appl. Mater. Interfaces* **2025**, *17* (8), 11522−11551.

(6) Chintersingh, K.-L.; Sun, Y.; Schoenitz, M.; Dreizin, E. L. Heterogeneous Reaction Kinetics for Oxidation and Combustion of Boron. *Thermochim. Acta* **2019**, *682*, No. 178415.

(7) King, M. K. Ignition and Combustion of Boron Particles and Clouds. *J. Spacecr. Rockets* **1982**, *19* (4), 294−306.

(8) Yeh, C. L.; Kuo, K. K. Ignition and Combustion of Boron Particles. *Prog. Energy Combust. Sci.* **1996**, *22* (6), 511−541.

(9) Huang, S.; Deng, S.; Jiang, Y.; Zheng, X. Experimental Effective Metal Oxides to Enhance Boron Combustion. *Combust. Flame* **2019**, *205*, 278−285.

(10) Sundaram, D.; Yang, V.; Yetter, R. A. Metal-Based Nanoenergetic Materials: Synthesis, Properties, and Applications. *Prog. Energy Combust. Sci.* **2017**, *61*, 293−365.

(11) Gottfried, J. L.; Wainwright, E. R.; Huang, S.; Jiang, Y.; Zheng, X. Probing Boron Thermite Energy Release at Rapid Heating Rates. *Combust. Flame* **2021**, *231*, No. 111491.

(12) Krier, H.; Burton, R. L.; Spalding, M. J.; Rood, T. J. Ignition Dynamics of Boron Particles in a Shock Tube. *J. Propul. Power* **1998**, *14* (2), 166−172.

(13) Jain, A.; Joseph, K.; Anthonysamy, S.; Gupta, G. S. Kinetics of Oxidation of Boron Powder. *Thermochim. Acta* **2011**, *514* (1−2), 67−73.

(14) Young, G.; Sullivan, K.; Zachariah, M.; Yu, K. Combustion Characteristics of Boron Nanoparticles. *Combust. Flame* **2009**, *156* (2), 322−333.

(15) Wang, Y.; Xu, F.; Issac Paul, G.; Vidales Pasos, E.; Shi, K.; Wagner, B.; Mangolini, L.; Zachariah, M. R. Role of Surface Tension

Downloaded from pubs.acs.org/aamick/article-pdf/18/46/63811/6913516/am-2026-13891b.pdf by UNIV OF CALIFORNIA RIVERSIDE user on 26 November 2026

on Heat Feedback and Power from Energetic Composites. *ACS Appl. Mater. Interfaces* **2024**, *16* (32), 42100−42108.
(16) Chowdhury, M.; Ghildiyal, P.; Rojas, A.; Wang, Y.; Wang, H.; Zachariah, M. R. High-Yield Spray Drying Assembly and Reactive Properties of Nanoenergetic Mesoparticle Composites. *Adv. Powder Technol.* **2023**, *34* (7), No. 104075.
(17) Wang, Y.; Chowdhury, M.; Zhou, Y.; Issac Paul, G.; Shi, K.; Zachariah, M. R. Oscillating-to-Continuous Combustion Transition in Mesoparticle Composites Through Manipulation of Heat Feedback. *Adv. Funct. Mater.* **2024**, No. 2406722.
(18) Wang, H.; Jian, G.; Egan, G. C.; Zachariah, M. R. Assembly and Reactive Properties of Al/CuO Based Nanothermite Microparticles. *Combust. Flame* **2014**, *161* (8), 2203−2208.
(19) Wang, H.; Jian, G.; Yan, S.; DeLisio, J. B.; Huang, C.; Zachariah, M. R. Electrospray Formation of Gelled Nano-Aluminum Microspheres with Superior Reactivity. *ACS Appl. Mater. Interfaces* **2013**, *5* (15), 6797−6801.
(20) Jacob, R. J.; Wei, B.; Zachariah, M. R. Quantifying the Enhanced Combustion Characteristics of Electrospray Assembled Aluminum Mesoparticles. *Combust. Flame* **2016**, *167*, 472−480.
(21) Wang, H.; Jacob, R. J.; DeLisio, J. B.; Zachariah, M. R. Assembly and Encapsulation of Aluminum NP's within AP/NC Matrix and Their Reactive Properties. *Combust. Flame* **2017**, *180*, 175−183.
(22) Wang, H.; Jian, G.; Zhou, W.; DeLisio, J. B.; Lee, V. T.; Zachariah, M. R. Metal Iodate-Based Energetic Composites and Their Combustion and Biocidal Performance. *ACS Appl. Mater. Interfaces* **2015**, *7* (31), 17363−17370.
(23) Cheng, L.; Yang, H.; Yang, Y.; Li, Y.; Meng, Y.; Li, Y.; Song, D.; Chen, H.; Artiaga, R. Preparation of B/Nitrocellulose/Fe Particles and Their Effect on the Performance of an Ammonium Perchlorate Propellant. *Combust. Flame* **2020**, *211*, 456−464.
(24) Hu, Y.; Wang, X.; Zhang, J.; Zhu, Z.; Ren, X.; Yang, Y.; Lin, K.; Pang, A.; Shuai, Y. Encapsulated Boron-Based Energetic Spherical Composites with Improved Reaction Efficiency and Combustion Performance. *Chem. Eng. J.* **2022**, *433*, No. 134478.
(25) Jain, S.; Mehilal, M.; Nandagopal, S.; Singh, P.; Radhakrishnan, K.; Bhattacharya, B. Size and Shape of Ammonium Perchlorate and Their Influence on Properties of Composite Propellant. *DSJ* **2009**, *59* (3), 294−299.
(26) Hedman, T. D.; Reese, D. A.; Cho, K. Y.; Groven, L. J.; Lucht, R. P.; Son, S. F. An Experimental Study of the Effects of Catalysts on an Ammonium Perchlorate Based Composite Propellant Using 5kHz PLIF. *Combust. Flame* **2012**, *159* (4), 1748−1758.
(27) Zhou, W.; DeLisio, J. B.; Wang, X.; Zachariah, M. R. Reaction Mechanisms of Potassium Oxysalts Based Energetic Composites. *Combust. Flame* **2017**, *177*, 1−9.
(28) Wu, T.; SyBing, A.; Wang, X.; Zachariah, M. R. Aerosol Synthesis of Phase Pure Iodine/Iodic Biocide Microparticles. *J. Mater. Res.* **2017**, *32* (4), 890−896.
(29) Chowdhury, M.; Wagner, B.; Wagner, Y.; Shi, K.; Tran, I.; Dickson, M.; Mongolini, L.; Zachariah, M. R. Energetic Characteristics and Reaction Mechanism of Hydrogenated Magnesium Nanoparticles: Role of Condensed Phase Reaction. *ACS Appl. Mater. Interfaces* **2025**, *17*, 21180.
(30) Jian, G.; Piekiel, N. W.; Zachariah, M. R. Time-Resolved Mass Spectrometry of Nano-Al and Nano-Al/CuO Thermite under Rapid Heating: A Mechanistic Study. *J. Phys. Chem. C* **2012**, *116* (51), 26881−26887.
(31) DeLisio, J. B.; Hu, X.; Wu, T.; Egan, G. C.; Young, G.; Zachariah, M. R. Probing the Reaction Mechanism of Aluminum/Poly(Vinylidene Fluoride) Composites. *J. Phys. Chem. B* **2016**, *120* (24), 5534−5542.
(32) Jian, G.; Chowdhury, S.; Sullivan, K.; Zachariah, M. R. Nanothermite Reactions: Is Gas Phase Oxygen Generation from the Oxygen Carrier an Essential Prerequisite to Ignition?. *Combust. Flame* **2013**, *160* (2), 432−437.
(33) Ghildiyal, P.; Ke, X.; Biswas, P.; Nava, G.; Schwan, J.; Xu, F.; Kline, D. J.; Wang, H.; Mangolini, L.; Zachariah, M. R. Silicon Nanoparticles for the Reactivity and Energetic Density Enhancement of Energetic-Biocidal Mesoparticle Composites. *ACS Appl. Mater. Interfaces* **2021**, *13* (1), 458−467.
(34) Xu, F.; Biswas, P.; Nava, G.; Schwan, J.; Kline, D. J.; Rehwoldt, M. C.; Mangolini, L.; Zachariah, M. R. Tuning the Reactivity and Energy Release Rate of I^2O^5 Based Ternary Thermite Systems. *Combust. Flame* **2021**, *228*, 210−217.
(35) Zhou, Y.; Shi, K.; Chowdhury, M.; Hagen, E.; Wang, Y.; Zachariah, M. R. Direct Microscopic Imaging of Exploding Aluminum/Nitrocellulose Mesoparticles to Reveal the Enhanced Combustion Mechanism. *Fuel* **2025**, *387*, No. 134348.
(36) Gurram, N.; Chakravarthy, S. R. Experimental Investigation of Cellular Instability in Ammonium Perchlorate (AP) and Fine AP-Binder Mixtures. *Proc. Combust. Inst.* **2015**, *35* (2), 2455−2461.
(37) Vyazovkin, S.; Wight, C. A. Kinetics of Thermal Decomposition of Cubic Ammonium Perchlorate. *Chem. Mater.* **1999**, *11* (11), 3386−3393.
(38) Johnson, G. K.; Hubbard, W. N. The Enthalpies of Formation of Crystalline and Amorphous Boric Oxide and Orthoboric Acid. *J. Chem. Thermodyn.* **1969**, *1* (5), 459−468.
(39) Xi, X.; Shufen, L. Generation of BN in the Combustion Residue of Boron-Containing Propellant. *J. Energ. Mater.* **2003**, *21* (1), 63−72.
(40) Góbi, S.; Bergantini, A.; Turner, A. M.; Kaiser, R. I. Electron Radiolysis of Ammonium Perchlorate: A Reflectron Time-of-Flight Mass Spectrometric Study. *J. Phys. Chem. A* **2017**, *121* (20), 3879−3890.
(41) Ao, W.; Wang, Y.; Wu, S. Ignition Kinetics of Boron in Primary Combustion Products of Propellant Based on Its Unique Characteristics. *Acta Astronaut.* **2017**, *136*, 450−458.
(42) Jiao, C. Q.; Nagpal, R.; Haaland, P. Ion Chemistry in Boron Trichloride BCl3. *Chem. Phys. Lett.* **1997**, *265* (1−2), 239−243.
(43) Jain, S.; Chakraborty, S.; Qiao, L. Burn Rate Enhancement of Ammonium Perchlorate−Nitrocellulose Composite Solid Propellant Using Copper Oxide−Graphene Foam Micro-Structures. *Combust. Flame* **2019**, *206*, 282−291.

Downloaded from pubs.acs.org/aamick/article-pdf/18/46/63811/6913516/am-2026-13891b.pdf by UNIV OF CALIFORNIA RIVERSIDE user on 26 November 2026

https://doi.org/10.1021/acsami.6c13891
ACS Appl. Mater. Interfaces 2026, 18, 63811−63820